Title
LOW-ALTITUDE TRAPPED PROTONS DURING SOLAR MINIMUM PERIOD 1962-1966

Authors
Heckman, Harry H.
Nakano, George H.

Publication Date
1968-09-01

UCRL-18422

cy. 2

LOW-ALTITUDE TRAPPED PROTONS DURING SOLAR MINIMUM PERIOD, 1962-1966

Harry H. Heckman and George H. Nakano

September 1968

LRL

LAWRENCE RADIATION LABORATORY
UNIVERSITY of CALIFORNIA BERKELEY

UCRL-18422
cy. 2

DISCLAIMER

Submitted to Journal of Geophysical Research

UCRL-18422
Preprint

UNIVERSITY OF CALIFORNIA

Lawrence Radiation Laboratory
Berkeley, California

AEC Contract No. W-7405-eng-48

LOW-ALTITUDE TRAPPED PROTONS DURING SOLAR MINIMUM PERIOD, 1962-1966

Harry H. Heckman and George H. Nakano

September 1968

LOW-ALTITUDE TRAPPED PROTONS DURING SOLAR MINIMUM PERIOD, 1962-1966

Harry H. Heckman

Lawrence Radiation Laboratory
University of California
Berkeley, California

and

George H. Nakano

Research Laboratories
Lockheed Missiles and Space Company
Palo Alto, California

September 1968

ABSTRACT

Observations of energetic protons in the inner radiation belt have been carried out since September 1962 with emulsion detectors recovered from polar-orbiting low-altitude satellites. Experimental results obtained between November 1962 and June 1966, during the period of minimum solar activity, are as follows:

(a) The omnidirectional proton flux at 63 MeV remained constant to within ±7.6 per cent, an error comparable to the statistical accuracy of the flux measurements.

(b) No detectable change in the energy spectrum above 57 MeV occurred. These results can be ascribed, qualitatively, to the concurrent minimum of solar activity and stability of the 10.7-cm uv flux, $\bar{F}$, during this period.

(c) The omnidirectional flux versus altitude profile can be fitted by a power-law function of altitude with exponent $n = 4.67 \pm 0.08$. This value

of n is in agreement with that deduced from measurement of the east-west asymmetries in the proton flux. The measured proton flux scale heights are significantly larger than can be accounted for by the Harris and Priester model atmosphere. Apart from effects due to sources other than albedo neutron decay, the data suggest either that errors exist in the model atmosphere, particularly in regards to the density gradient, or that adiabatic particle motion is violated.

INTRODUCTION

Between September 1962 and June 1966, nuclear emulsion particle detectors were successfully recovered from 30 earth-oriented satellites after 2 to 7 days in polar orbit. Of these recoveries, 27 yielded useful experimental data on the spatial and temporal properties of energetic trapped protons at low satellite altitudes. This paper reports the results of these experiments, which pertain to inner-radiation belt protons detected in the region of the South Atlantic anomaly during the recent period of minimum solar activity.

Partial results obtained from flights prior to September 1963 have been published previously [Heckman and Nakano, 1963 and 1965]. All data reported here have been analyzed in common. The present analysis follows closely that given previously, but has been augmented and refined in many of its details. Important to this study is that all experiments were performed under conditions that were, for practical purposes, identical. The emulsions were mounted on the vehicle, in a reproducible and known geometry, the vehicle was earth-oriented at all times, and its orientation could be, and was, independently verified from our own measurements. Orbit inclinations were from 64.9° to 115.0°, and the ascending-node altitudes were between 245 and 519 km at the center of the South Atlantic anomaly.

Quantities that we have examined for evidence of temporal variations during the approximately 4-year period are the omnidirectional proton flux, east-west asymmetry of the proton flux, and energy spectrum. The altitude dependence of the proton flux and the east-west asymmetry of this flux

have also been obtained. Between September 1962 and June 1966 we find no evidence for significant changes in the character of the trapped high-energy protons. With the exception of our first flight (September 1962), the proton flux at 63 MeV has remained constant to within ±7.6 per cent--an error that is comparable to the statistical accuracy of measurement. No changes in the shape of the energy spectrum for $E > 57$ MeV have been detected. Within the range of altitudes examined the east-west asymmetries and the profile of altitude vs flux cannot be fully accounted for by atmospheric losses, as deduced from model atmospheres, under the assumption of adiabatically conserved particle motion.

EXPERIMENTAL CONFIGURATION

A. Orbit Parameters and Satellite Orientation

All satellites were launched into near-polar orbit, with apogee usually occurring in the southern hemisphere in the ascending node, i.e., while the satellite was traveling northward. Ephemeris data listed for each flight the altitude, latitude, and longitude of the satellite at 1-minute intervals. The locations of the satellites were known to within ±1 km. Attitude control was maintained at all times in order to orient the orbiting vehicle relative to the velocity and zenith vectors.

B. Emulsion Detectors

Four small "button-shaped" stacks of nuclear track emulsions, each 4 cm in diameter by 0.48 cm thick, were used on each flight. The emulsion stacks consisted of four pellicles of Ilford G.2, 600 μ thick, and eight pellicles of Ilford G.5, 300 μ thick. These emulsions have identical chemical composition, differing only in their sensitivity.

Type G.2 is sensitive to singly charged particles, $\beta \lesssim 0.4$, whereas type G.5 is electron-sensitive, hence capable of recording relativistic particles.

C. Orientation of Emulsion

The emulsion stacks were placed in stainless steel canisters and mounted on a spherical ballast shell immediately behind the ablative shield of the recoverable section of the satellite. The geometrical configuration of the emulsion detectors in the nose cone was accurately known. As a result, the emulsions were uniquely oriented during flight with respect to the spacecraft's orbital velocity and zenith vectors. Figure 1 is a near-vertical photograph of the emulsion detectors before their removal from the ballast shell after recovery. The $\hat{i}\hat{j}\hat{k}$ coordinate system indicated is fixed in the satellite. During flight, the vector $\hat{i}$ is directed toward the zenith, i.e., normal to the earth's surface. The vector $\hat{k}$ is the axis of symmetry of the satellite, which, for these experiments, was aligned antiparallel to the orbital velocity vector, $\hat{v}$.

Figure 1 portrays a common flight configuration. The angle between $\hat{k}$ and the normal to the emulsions is 36°. Counterclockwise from $\hat{i}$ the azimuthal angles of the detector positions are 48.5°, 118°, 270°, and 312°. That the emulsions were spatially oriented during their irradiations to the trapped radiation is the most significant operational feature of the experiment--one that simplified the methods for scanning the emulsions as well as the analysis and interpretation of the data.

D. Shielding

The exposure geometry as described above allows for the detection of particles over a 2π solid angle at each detector position. Particles within this solid angle enter the upper surface or edge of the stacks after penetrating the ablative shielding and canister. The ablative shield is a laminated structure of phenolic glass and nylon phenolic whose thickness depends on direction. The minimum thickness of 2.48 g/cm^2 is in the direction normal to the detector surfaces. The minimum detectable energy for protons (including the energy loss in the canister) is 57.3 MeV. Protons that enter the emulsions parallel to the emulsion surface have cutoff energies between 70 and 106 MeV, depending on the direction of incidence.

TOPOLOGY OF MIRRORING PROTONS IN THE SOUTH ATLANTIC ANOMALY

Because of the low satellite altitudes at which these experiments were performed, the detection of trapped radiation was confined to the South Atlantic anomaly, a region of enhanced trapped radiation where the inner Van Allen belt particles attain their minimum mirror-point altitudes. The dominant feature of the trapped radiation in the anomaly region is its planar geometry. The radiation is most intense in the plane normal to the local magnetic field. Particles that are not normal to the magnetic field at the point of observation are mirrored at lower altitudes and are rapidly attenuated owing to their increased penetration into the atmosphere. The pitch-angle distribution about the mirror plane is therefore sharply defined. An effective atmosphere of constant scale height, H, for example, produces a Gaussian distribution of pitch angle. (See Appendix I.)

At 400 km altitude, $H \approx 80$ km and the calculated standard deviation, σ, of the pitch angle distribution relative to the mirror plane is $\pm 8.6°$, consistent with observation [Heckman and Nakano, 1963; Filz and Holeman, 1965].

That the mirror geometry of the trapped radiation is observable in the emulsion detectors is attributable to the fact that the radiation is detected only in the relatively small geographic area of the South Atlantic anomaly. Further, the orientations of the mirror plane recorded in the emulsion detectors during ascending and descending nodes of the orbit are clearly resolved from each other (Figure 2). The relative orientation of the mirror plane is a result of rotation about the satellite's $\hat{i}$ axis by the amount $R_i = 180° + 2\omega$, where $\omega = \sin^{-1}(\frac{\cos\Omega}{\sin\theta})$, Ω is the orbit inclination, and θ is the colatitude of the observation point.

Figure 2 illustrates the geometric orientation of the planes of mirroring protons as recorded by the emulsion detectors in flight configuration when the orbit inclination is 75°. The illustration shows the mirror planes as they would appear at the site of maximum proton intensity in the anomaly region ($\approx$34° W, 34° S), and is representative of the mean orientation of these planes recorded by the detectors. The observed angular width of the mirror planes is determined predominantly by (a) the intrinsic pitch-angle distribution of the protons and (b) the broadening of this distribution by the precession of the magnetic field vector during the orbital traversals of the anomaly region as seen in the $\hat{i}$, $\hat{j}$, $\hat{k}$ (satellite) frame. The precession of the field vector in the $\hat{i}$, $\hat{j}$, $\hat{k}$ system is a composite motion due to the variations in the vector directions of $\underset{\sim}{B}$ within the anomaly region and the relative motion between the $\hat{k}$ axis of the satellite and true north, $\hat{n}$,

as each traversal of the anomaly is made. (For a circular orbit, the angle between $\hat{k}$ and $\hat{n}$ is ω, defined above, and its rate of change is $\dot{\omega} = \dot{\alpha} \cos\Omega \cos\theta/\sin^2\theta$, where $\dot{\alpha}$ is the orbital angular velocity.) We have calculated the rms broadening, σ_b, of the pitch angle distribution in the plane of the emulsion, stack A, due to the precession of $\underset{\sim}{B}$, and find $\sigma_b \approx 10°$. We have consistently found rms widths of the mirror planes to be $\sigma_{meas} \approx 13°$ [Heckman and Nakano, 1963]. Given $\sigma_b \approx 10°$, we obtain $\sigma \approx 8°$ as the width of the intrinsic pitch angle distribution, in agreement with the computational results in Appendix I.

EXPERIMENTAL RESULTS

Verification of Orientation

The first step in our analysis was to determine the mirror-plane configuration recorded in each emulsion stack. The configuration of the mirror planes observed in each emulsion detector is dependent upon the position of the detector on the ballast shell, the orbital inclination, and the orientation of the satellite relative to the local magnetic field in the region where the mirroring particles are detected. We take the normal to the mirror planes to be the mean direction of the magnetic field vector over the mirroring region as observed in the $\hat{i}\hat{j}\hat{k}$ reference frame of the satellite. A possible mirroring region is found whenever the magnetic field vector in the satellite reference frame, upon being transformed to earth-centered polar coordinates at the geographic point under consideration, aligns with the earth's field as given by the Jensen and Cain [1962] 48-term field expansion.

Additional information is obtained from the observation of the east-west asymmetry in the proton flux. Because the unidirectional flux, $\underline{j}_{east}$, is greater than $\underline{j}_{west}$, the east-to-west direction at the time of exposure can be determined. The orientation of the satellite's $\hat{\underline{j}}$ axis with respect to the east-west direction that is obtained via particle asymmetry measurements establishes the vector direction of $\underline{B}$ and restricts the mirroring region to the southern hemisphere. Here, there are two possible sites, both in the South Atlantic Ocean; one near South America, the other near Central Africa. From geometrical considerations alone, these sites are indistinguishable. The magnitudes of the magnetic field in these regions, however, are not equal. The lower field intensity over the South American site identifies this particular area as the mirroring region. We have, in other words, deduced that the trapped particles we observe in the emulsions were detected in the well-known South Atlantic anomaly.

The results of the geometrical analysis described above are given in Figure 3 for a representative sample of the flight experiments. Each datum point corresponds to an individual flight. The data identify well the central region of the South Atlantic anomaly--the clustering of points attests to the excellent reproducibility of the experimental configuration and attitude control of the satellite. The error bars represent the statistical accuracies in our determinations, based on the measurement errors of the magnetic inclination (vertical bars) and declination (horizontal bars) angles. The distribution in the values of the magnetic inclination, I, is consistent with the measurement errors alone, and indicates that the errors in satellite orientation relative to the zenith direction is less than our measurement error of $\pm 2^\circ$. The distribution in the declination angles

suggests on the other hand, that the attitude-control error in yaw could be as high as ±3°. By the foregoing analyses, we verified that each flight experiment was properly executed under the nominal operational conditions.

East-West Asymmetry

The east-west asymmetry in the directional flux of energetic trapped protons [Lenchek and Singer, 1962] is clearly observed at low satellite altitudes in the South Atlantic anomaly [Heckman and Nakano, 1963; Galperin and Temny, 1965; and Filz and Holeman, 1965]. That an east-west flux asymmetry is a general feature of inner belt protons is supported by the Explorer 11 satellite observations by Garmire [1963].

An asymmetry in the proton flux will appear wherever a flux gradient exists, irrespective of the physical phenomena that generate the gradient [Northrop, 1963]. At the inner edge of the radiation belt, it is the atmospheric density gradient that produces the flux gradient and thus the east-west asymmetry. The trapped radiation penetrates the atmosphere to its greatest extent while traversing the South Atlantic. Thus, the effective atmospheric density experienced by a trapped particle during its longitudinal drift period is largely determined in this region. At altitudes up to about 400 km, scale heights of the effective atmospheric density averaged over the particle's motion are only slightly greater (by 25 per cent and less) than the scale height of the atmosphere at the particle's minimum mirror-point altitude, h_{min} [Heckman and Brady, 1966]. Measurements of proton flux scale heights via east-west asymmetry measurements in the anomaly thus can be directly compared with model atmospheric scale heights. This is done in Figure 4a.

The calculational results of Heckman and Brady [1966] show that within the range of altitudes we are considering the effective atmospheric density scale height is not constant, but increases approximately in proportion to altitude. The proportionality factor depends on, and increases with, solar activity, and is demonstrated in Figure 4a. The effective atmospheric density thus has an altitude dependence that is more nearly a power law than exponential.

In order to present the proton flux east-west asymmetry data as scale heights, we therefore assume the altitude profile of the directional proton flux to be a power law. In terms of the $\underline{j}_E : \underline{j}_W$ flux ratios, the proton-flux scale height is given by

$$H = h \, \ell n \left[\frac{1+\Delta h/h}{1-\Delta h/h}\right] \Big/ \ell n \, \frac{\underline{j}_E}{\underline{j}_W} , \qquad (1a)$$

and the power-law exponent, n, is

$$n = h/H. \qquad (1b)$$

In the above expression, the quantity $\Delta h = a \cos I \cos \phi$ is the difference in altitude between the point of observation, h, and the guiding centers of $\underline{j}_E$ and $\underline{j}_W$, where $a = pc/B$ is the gyroradius of the particle, I is the dip angle of the magnetic field, and ϕ is the angle between $\hat{\underline{B}} \times \hat{\underline{r}}$ (where $\hat{\underline{r}}$ is the zenith vector) and the direction along which the asymmetry measurements are made. In these experiments, the east-west asymmetry was measured at a mean proton energy of 132 MeV (a = 78 km for B = 0.22 gauss), with $0.439 \leq \cos \phi \leq 0.961$, depending upon orbit inclination. The average magnetic dip angle at which the measurements were made was $I = 42°$.

The errors assigned to the flux asymmetry data include the statistical uncertainty of the measured east:west ratio, the error in the background correction to the ratio, and the error due to uncertainties in the geometrical configuration. Combining the aforementioned errors leads to overall fractional errors in our scale-height measurements that average ±11 per cent, with a maximum of 23 per cent for the lowest-altitude point.

The east-west asymmetries were measured by counting the number of stopping protons in the energy interval 132 ± 10 MeV that enter diametrically opposite edges of the stack A (see Figure 2). To be counted, the direction of a proton track 1 mm from its ending had to be within ±15° of the ascending-node mirror plane and ±10° to the plane of the emulsion.

The principal source of background to the east-west ratios originated in the ablative shielding over the emulsions owing to scattering and secondary-particle production by the trapped radiation and primary cosmic rays. The correction for this background was estimated by counting the number of stopping protons having the same angular criteria as above, but whose incident directions eliminated them as constituents of the trapped radiation.

The altitude assigned to each experimental point is $\overline{h}_{min}$, the flux-weighted average minimum mirror-point altitude for that particular satellite flight (see Appendix II for a definition of $\overline{h}_{min}$), less a correction of ϵ = 16 to 18 km, depending on altitude. This correction comes about because the east-west asymmetry is measured over a finite range of pitch angles about the mirror plane, e.g., $\delta_{meas} = \pm \pi/12$, rather than strictly normal to the magnetic field. The altitude ϵ is given to good approximation by $\epsilon = 2.0 \times 10^3 \langle \delta^2 \rangle$, where $\langle \delta^2 \rangle$ is the square of the intrinsic pitch angle up to which the measurements were taken, averaged over the local pitch-

angle distribution.

The asymmetry data shown in Figure 4a present the dependence of the proton flux scale height on altitude; Figure 4b gives the corresponding values of the exponent n. The mean value of n deduced from the particle asymmetry data is $\bar{n} = 4.93 \pm 0.12$. Also shown in Figure 4a is H vs $\bar{h}_{min}$ for n = 4.67, the exponent that is derived from the altitude profile of the omnidirectional flux of 63-MeV protons. These latter data are presented in the following section. The proton flux scale-height data are compared with curves of energy-loss scale heights vs altitude that are appropriate for atmospheres at solar minimum (S = 100) and solar maximum (S = 200). The curves of H vs $\bar{h}_{min}$ are those given by Heckman and Brady [1966], who computed the effective atmospheric scale heights for 125-MeV protons, $0.204 \leq B \leq 0.236$, L = 1.38. The Harris and Priester [1962] model atmosphere was used in the computations, and the effective atmospheric densities and energy loss and their scale heights were found by averaging these various quantities over the particle's trajectory.

Proton Flux Measurements

Scanning Procedure

The proton flux was determined by sampling the areal density of normally incident protons that stopped in emulsion stack A. The energy increment over which the flux measurements were made was $57.3 < E < 68.2$ MeV ($\bar{E}$ = 63 MeV). Again referring to Figure 2, we note that the ascending-node mirror plane is nearly normal to the emulsion plane of stack A. (The angle between the mirror and emulsion planes varies slowly with orbit inclination, Ω. As illustrated in Figure 2, the mirror-emulsion plane angle is 92° when Ω = 75°.)

In order to demonstrate the scanning geometry and angular selection criteria, we schematically show in Figure 5 how the emulsion is oriented during the course of this analysis. Preceding the flux measurements, the orientation of the ascending-node mirror plane in the emulsion and the east-west asymmetry of the flux are determined. The emulsion is placed on the microscope stage so that the intersection of the mirror and emulsion planes is parallel to the x axis, and given the east-west asymmetry, the earth's magnetic field vector is aligned along the y axis. The mirror plane is then confined to the x-z plane to within a few degrees, where the z axis is the optical axis of the microscope.

Vector $\underset{\sim}{P}$ represents the direction of an incident stopping proton measured at the surface of the emulsion. A proton is counted when the projected angle of $\underset{\sim}{P}$ on the mirror plane, ϕ_P, satisfies the criterion

$$\phi_P \leq \tan^{-1} \frac{x_P}{z_P} = \pm 15^\circ .$$

The mean angle in the mirror plane at which the vertically incident flux is observed is $25^\circ < \phi_v < 74^\circ$, depending on orbit inclination. The "east-west" vector, $\hat{\underset{\sim}{B}} \times \hat{\underset{\sim}{r}}$, defines the direction $\phi = 0$.

Omnidirectional Flux vs Altitude

The quantity actually measured in our scanning procedure is the directional flux of protons at angle ϕ_v in the mirror plane. As evidenced by the east-west asymmetry, the directional flux is not azimuthally uniform in the mirror plane. This is taken into account when the data are transformed from directional to omnidirectional proton flux in the following manner: Under the assumption that the altitude profile of the directional proton flux is a power law, $j(\phi)$ can be expressed as

$$j(\phi) = (1 + \frac{a}{h} \cos I \cos \phi)^n. \qquad (2)$$

The factor F, which converts the directional flux to omnidirectional flux, is then

$$F = \frac{\int_0^{2\pi} (1 + \frac{a}{h} \cos I \cos \phi)^n \, d\phi}{j(\phi_v)\,\Delta\phi}$$

$$\approx \frac{2\pi\left[1 + \frac{n(n-1)}{4}\left(\frac{a \cos I}{h}\right)^2 + 0\left(\frac{a \cos I}{h}\right)^4 + \cdots\right]}{j(\phi_v)\,\Delta\phi}, \qquad (3)$$

where

$n \approx 5$, as obtained from the asymmetry data;

$j(\phi_v)$ is the directional flux observed at ϕ_v;

and $\Delta\phi$ is the angular interval in the mirror plane in which the directional flux is measured.

Typically, $\Delta\phi = \pi/6$ radians.

In our experiments, $(a/h)\cos I$ is about 0.1, and F may vary between 7.8 (when $\cos \phi_v = 1$) and 21.3 (when $\cos\phi_v = -1$) when $\Delta\phi = \pi/6$. We note that F = 12 for an azimuthally uniform distribution of flux in the mirror plane, i.e., when n or $a \to 0$.

Figure 6 presents our measurements on the altitude dependence of the omnidirectional flux of $\bar{E}$ = 63 MeV protons. Plotted is the average daily integrated flux, J (in units of cm^{-2} MeV^{-1} day^{-1}), observed for each satellite flight, versus the average minimum mirror-point altitude, $\bar{h}_{min}$. Each datum point was measured to a statistical accuracy of ±5 per cent. The data are all normalized to a 90° orbit inclination because

the integrated proton flux detected during a 24-hour period at a constant satellite altitude varies with orbit inclination. Based upon our calculation using Injun 3 proton data, we find that the daily integrated proton flux at 63 MeV increases approximately linearly with the angle $|90° - \Omega|$ for $65° < \Omega < 115°$. Specifically, the expression we used to normalize the flux data to a 90° orbit is $J(\Omega) = [1 + 0.0065|90 - \Omega| J(90°)]$, where $J(\Omega)$ is the daily integrated flux observed at orbit inclination Ω. The altitude dependence of this normalization factor is small [Vette, 1966], and no correction was made. The normalization of the flux data to J(90°) reduced the scatter of the data about the least-squares adjusted power-law fit from a standard deviation of ≈10 per cent to 7.6 per cent. Our final result is that the exponent of the power-law relationship between J(in $cm^{-2}MeV^{-1}day^{-1}$) at 63 MeV and $\overline{h}_{min}$ is $n = 4.67 \pm 0.08$.

Also shown in Figure 6 are the values computed for the daily flux of 63-MeV protons for each flight by using the ephemeris data, the Jensen and Cain [1962] 48-coefficient spherical harmonic expansion of the geomagnetic field, and the Injun 3 proton data [Valerio, 1964, and Peterson, 1966]. In order to deduce J(63 MeV) from the Injun 3 measurements, $40 < E < 110$ MeV, we assumed the differential energy spectrum in this energy interval to be exponential, of the type

$$J \propto \exp[-E/E_0(L)],$$

where the L dependence of E_0 is that given by McIlwain and Pizzella [1963]. Although there is evidence that the characteristic energy E_0 is also a function of B [Freden, Blake, and Paulikas, 1965], the information presently available on this is not extensive enough to permit us to include this refinement in our flux computations.

The original purpose for computing the Injun 3 daily flux was to compare the ratio $J_{obs}/J_{Inj\ 3}$ in order to estimate variations in the flux data owing to differences in orbit inclination, eccentricity, etc. However, as these data accumulated, it became apparent that the ratios $J_{obs}/J_{Inj\ 3}$ varied systematically with altitude, and therefore could not be used directly to correct for orbit-dependent differences. Referring to Figure 6, we note the Injun 3 flux agrees very well as to absolute flux, but has an exponent $n_{Inj\ 3} = 4.05 \pm 0.04$, which is significantly less than the $n = 4.67 \pm 0.08$ obtained in the present experiment. We note that the scatter of the daily flux values about $J_{Inj\ 3}$ is small, about ±3 per cent (SD). A scatter in flux data of this amount can be accounted for by a random error of only ±2 km in calculating $\bar{h}_{min}$. Computations using the 1964-45A [Freden, Blake, and Paulikas, 1967] and Telstar I [Gabbe and Brown, 1966] flux contours give equally precise power-law altitude-flux profiles. The power-law exponents are in good agreement with each other ($n_{1964\text{-}45A} = 4.04 \pm 0.03$, $n_{Telstar\ I} = 3.96 \pm 0.07$). However, both the 1964-45A and Telstar I flux contours predict daily fluxes that are ≈ 30 per cent less than those given by Injun 3, hence, some 30 per cent less than the fluxes observed in this experiment.

In Figure 4a we have plotted particle scale heights vs $\bar{h}_{min}$ for the exponents n derived from the (unidirectional) east-west asymmetry and omnidirectional flux measurements. We wish to point out that these power-law exponents are, with small error, equal; hence, direct comparison of these quantities is justified.

On the basis of the east-west asymmetry data, we may express the unidirectional flux of particles normal to the local magnetic field as

$$\underline{j}_{\perp}(h, \phi) = [h + \Delta h]^{n} = h^{n}\left[1 + \frac{a \cos I}{h} \cos \phi\right]^{n}, \qquad (4)$$

where h is the detector altitude and $[h + \Delta h]$ is the altitude of the particles' guiding center. Following Farley and Sanders [1962], the omnidirectional flux at altitude h, J(h), is given by the integral equation

$$J(h) = 2\int_{0}^{2\pi} d\phi \int_{0}^{\delta_{max}} \underline{j}_{\perp}(h, \phi) \cos \delta \, d\delta. \qquad (5)$$

By (a) expanding $\underline{j}_{\perp}(h, \phi)$ in terms of a binomial series, (b) using the mirror equation $B/B_{mirror} = \cos^{2}\delta$, and (c) noting that $h = kB^{-6}$ at low altitudes in the anomaly region, equation 5 can be easily integrated to find J(h). Given that we express J(h) in the form $J(h) \propto h^{n'}$, we obtain the result that the difference between the exponents $n' - n \approx 0.02$ for the parameters in this experiment. This difference is therefore sufficiently small to justify equating n' to n.

Energy Spectrum

At least once per year during the solar minimum period we undertook a measurement of the proton energy spectrum E>57 MeV. As described in the previous section, vertically incident, stopping protons are limited to the energy interval $57.3 < E < 68.2$ MeV. Protons that enter parallel to the emulsion surface have a minimum cutoff energy of about 110 MeV. By utilizing both range and ionization measurements, the energy spectrum can be extended to ≈ 550 MeV, at which point the cosmic-ray background intensity becomes dominant.

Calibration: The ionization (i.e., grain density, g) versus velocity calibrations of the electron sensitive emulsions were obtained from stopping

proton tracks ≈ 1 cm in length. The ranges of the calibration protons were limited because the high particle intensities accumulated during a several-day flight (a) necessitated the use of thin emulsions ($\leq 300\ \mu$), and (b) disallowed the tracing of particle tracks to adjacent sheets. Grain density measurements were therefore carried out up to $\beta \approx 0.31$ (50 MeV) only. In order to extrapolate the g-vs-β curve to higher velocities, we took the shape of the g-vs-β curve given by Patrick and Barkas [1962], and normalized this curve to our measurements for $\beta \leq 0.31$.

Measurements: The procedures we used to determine grain densities followed that given by Barkas [1963]. Because of limited track lengths available for ionization measurements we utilized both the gap-length and blob-length structure of the track segments to give independent estimates of g. By doing so, we were able to attain statistical accuracies of ±5 per cent in g for track segments 300 to 1000 μ in length, depending on the level of ionization of the track. Accepted for ionization measurements were protons incident upon stack A whose projected directions were within ±10° of the mirror plane and whose dip angles were ≤ ±5° to the emulsion plane.

Results: Figure 7 presents proton spectra, E > 57 MeV, measured upon five different occasions between June 1963 and June 1966. The omnidirectional flux that is quoted is obtained from the observed sum of the eastward and westward directional fluxes following the procedures given in the previous section. Background corrections have been taken into account. By measuring the flux and ionization of particles not contained in the mirror planes of the trapped particles, we find that for energies less than 200 MeV

backgrounds are ≤ 10 per cent. Above this energy, the background level increases until at ≈550 MeV it amounts to about 55 per cent of the observed flux.

The spectra are all normalized to an altitude $\overline{h}_{min}$ = 375 km, assuming the power-law relationship $J \propto \overline{h}_{min}^{4.67}$ is valid for all energies. The scatter of flux values is largely due to the statistical accuracy of the measurements, i.e., typically ±15 per cent between 110 and 250 MeV, the data becoming statistically limited at the highest energy, where the errors can exceed ±50 per cent.

For comparative purposes, the dashed line through the data is a smooth curve drawn through the results of Heckman and Armstrong [1962]. These spectral data were taken in 1960 on an Atlas missile in ballistic trajectory (1185 km apogee) between Cape Kennedy and Ascension Island. The 1960 spectrum is arbitrarily normalized at 63 MeV, and demonstrates that little, if any, difference exists between that measurement, made near solar maximum at $\overline{h}_{min} \approx 550$ km, and the spectra observed in this experiment.

DISCUSSION OF RESULTS

As a basis for discussion, we recapitulate the pertinent results of this experiment, based on data obtained between November 1962 and June 1966, a period of very stable conditions. These results are compared with data obtained before and after the stable period and with calculations based on the Harris and Priester atmospheric model.

a. Between November 1962 and June 1966 inclusive, the omnidirectional flux of 63-MeV protons remained constant to within ±7.6 per cent, an error comparable to the statistical accuracy of the measurement, and no detectable change in the proton energy spectrum has been observed.

Long-term temporal variations in the proton flux are attributable to solar cycle changes in the upper atmosphere [Blanchard and Hess, 1964]. Variations in the solar uv heating of the upper atmosphere result in corresponding changes in the integrated atmospheric density traversed by trapped particles. During a period of minimum solar activity, trapped particles experience a less dense atmosphere. Hence, the proton flux is expected to achieve its maximum value at this time. Although the proton flux appears to have reached its maximum value during the recent period of low solar activity, the flux was actually observed to remain constant to within ±7.6 per cent. The high stability of the omnidirectional proton flux between November 1962 and June 1966 can be, to a large extent, ascribed to the concurrent stability of the monthly averaged 10.7-cm uv flux, $\overline{F}$ (in 10^{-22} W m^{-2} Hz^{-1}). In terms of the Harris and Priester model atmosphere [Harris and Priester, 1962 and 1963], the observed variations in $\overline{F}$ during this period result in density changes of the order of 10 per cent at the altitudes of interest. On this basis, one would expect very little change in the proton flux between 1962 and 1966, which concurs with our observations.

Any observation of natural monotonic variation in the proton flux just prior to the stable period were precluded by a rather severe transient perturbation produced by the Starfish nuclear detonation of July 1962.

Filz and Holeman [1965] observed the flux of 55-MeV protons from a series of experiments, similar to ours, aboard polar-orbiting satellites dating back to 1961. Following Starfish, Filz and Holeman detected a precipitous order-of-magnitude increase in the low-altitude proton flux, after which the proton intensity underwent decay. At the time of our first measurement, 8 weeks after Starfish, the proton flux at 63 MeV was about 40 per cent greater than the subsequent level of flux we were to observe throughout the solar-minimum period. By November 1962, the flux transient was no longer evident in our data, although this decay may have masked the detection of any natural flux variation through mid-1963 [Nakano and Heckman, 1968].

The solar minimum flux level was approximately twice that observed by Filz and Holeman [1965] during the 1961-1962 pre-Starfish period. Since the end of the solar minimum period (June 1966), we have observed a steady decrease in the proton flux. As of November 1967, the flux appears to be about one-half of the solar minimum flux level, a change that is significantly less than expected on the basis of the Blanchard and Hess calculations [Nakano and Heckman, 1968].

The spectral shape we have measured is in good agreement with those measured in 1959-1960 [Freden and White, 1959, 1960, 1962; Armstrong, Harrison, Heckman, and Rosen, 1961; and Heckman and Armstrong, 1962], irrespective of the fact that these latter experiments were carried out near solar maximum ($\overline{F} \approx 200$) at altitudes $460 < \overline{h}_{min} < 570$ km, some 100 to 200 km higher than the present satellite experiments. It should be pointed out, however, that solar-cycle changes in the energy spectrum, $E > 50$ MeV, diminish rapidly with increasing altitude [Blanchard and Hess, 1964], and the energy spectrum thus tends

toward temporal stability. We are then, in essence, comparing spectra observed during the solar minimum period with one that is more typical of a solar-cycle average. Solar-cycle differences between the spectra will be somewhat reduced, but certainly not eliminated.

b. The flux-vs-altitude profile is accurately expressed by the power-law function $J(63\ \text{MeV}) \propto \bar{h}_{min}^{n}$, where $n = 4.67 \pm 0.08$.

The long period of stability in the flux and energy spectrum made it possible to generate a precise flux-vs-altitude profile appropriate to the solar-minimum period. In addition, this stable period afforded us the opportunity to establish the reproducibility and internal consistency of the flux measurements, thereby lending credibility to the observed profile. This profile is accurately represented by a power-law function of $\bar{h}_{min}$, with the exponent $n = 4.67 \pm 0.08$.

We wish to compare this power-law exponent with those obtained by Filz [1968]. Based on data beginning in mid-1961, Filz finds that the flux-altitude exponent, n, was constant, and about 4.8, for all periods except one month after Starfish and in 1966. Of particular interest is the observation that, before Starfish, between August 1961 and June 1962, the slope of the power-law fit to the flux data was 4.79 [Filz and Holeman, 1965], the same as observed throughout the period late 1962 to mid 1966. Thus, although the plateau of the solar minimum flux was typically 100 per cent greater than the pre-Starfish flux, the altitude-vs-flux profile has remained the same. In other words, whereas the flux changes that have been observed are indicative of change in the average atmospheric density, we have no evidence for solar-cycle variations in the gradient of the atmosphere upon which the exponent n is expected to depend.

c. A less precise, though direct, measure of the power-law exponent n is obtained from the east-west asymmetry measurements, which yield a value $n = 4.93 \pm 0.12$.

Direct determinations of n, hence the particle scale heights, H, via the east-west asymmetry data are in agreement with the results obtained from the flux-vs-altitude profile cited in b. In Figure 4a we have intercompared these measured scale-height data, plotted as a function of altitude, with the omnidirectional flux data and with the effective scale heights expected on the basis of the Harris and Priester [1962] atmospheric model and the Jensen and Cain [1962] 48-term expansion of the geomagnetic field. Heckman and Brady [1966] computed the effective atmospheric densities and scale heights for 125-MeV protons in the South Atlantic anomaly, which may be directly compared with the 132-MeV proton asymmetry measurements made here. The striking feature of Figure 4a is that the scale-height data are characteristic of an atmosphere at times of maximum solar activity (S = 200), rather than at the time of minimum activity (S = 100) during which these data were actually taken. Because the characteristic lifetime of these protons is generally shorter than the prevailing 3.5 years of stable atmospheric conditions, it would appear that ample time was available for the protons to come to equilibrium with a solar-minimum-like atmosphere, such as labeled S = 100 in Figure 4a. (For a solar minimum atmosphere, the average resident time or "age" of a 132-MeV proton at 400 km altitude is typically 5 years; at 250 km less than 3 months.)

Apart from invoking particle sources other than albedo neutron decay to account for the large particle-scale heights, this result suggests

either that substantial errors exist in the model atmosphere, particularly in regard to the density gradient, or that the adiabaticity of motion of the energetic protons is violated. Of course, atmospheric models are not so firmly established as we would like. However, recent satellite drag data [King-Hele and Hingston, 1968 a, b] have tended to confirm the general features of the COSPAR International Reference Atmosphere 1965, i. e., the Harris and Priester model atmosphere, and rather severe modifications of this model would be required to rectify the discrepancy.

If we assume the model atmosphere is reasonably accurate, then the result shown in Figure 4a suggests that the particles are not indigenous to the altitude at which they are detected. That is to say, the enlarged particle scale heights could be accounted for if the trapped particles had previously experienced greater atmospheric scale heights. Such scale heights are encountered at higher altitudes. Hence, these data provide circumstantial evidence for the diffusion of energetic protons in B or L. The net result of such an effect would be to give larger particle scale heights, and would diminish the effects of atmospheric solar-cycle changes in the altitude profile and spectral shape. In addition, B or L diffusion would yield proton fluxes greater than those expected from simple atmospheric losses alone under the assumption of adiabatically conserved particle motion. It was to the latter problem that Dragt, Austin, and White [1966] addressed themselves in their work on the probabilities for the injection of protons into the radiation belt by albedo neutron decay. They concluded that the observed flux of trapped inner-belt protons with energies >20 MeV are larger by a factor of ≈ 50 than can be reasonably explained by the albedo neutron hypothesis and atmospheric losses alone.

Dragt et al., proposed the possibility for pitch-angle diffusion, through the violation of the first adiabatic invariant, as a means to rectify this discrepancy. Such diffusion in pitch angle could be effected by hydromagnetic waves of sufficient amplitude at a frequency ($\approx$ 10 Hz) required for a resonant interaction [Dragt, 1961]. The interaction of high-energy protons with hydromagnetic waves at low L values and the resultant pitch-angle diffusion have yet to be established, but it is clear that such phenomena should be considered as a possible means to account for the apparent discrepancies, high fluxes and large scale heights. A consequence of such pitch-angle diffusion would be to diminish the solar-cycle variations of the inner-belt protons.

Acknowledgments. We thank the members of the Visual Measurements group of the Lawrence Radiation Laboratory, who assisted us in the analysis of the emulsion plates. Mr Thomas Coen of the Technical Photography Group assembled and processed the nuclear emulsions. We commend him for giving us a consistently excellent processed emulsion. We appreciate the many contributions of Mr. P. J. Lindstrom in carrying out the computer operations. Dr. Martin Walt's comments on this paper were particularly helpful. This work was carried out under auspices of the Atomic Energy Commission and of the Lockheed Missiles and Space Company, Independent Research.

APPENDIX I. Pitch Angle Distribution at Low Altitudes

Assuming that the mirror-point density along a magnetic field line between ℓ and $\ell + d\ell$ is inversely proportional to the effective atmospheric density $\rho(\ell)$, we wish to calculate the pitch-angle distribution $f(\delta)$, where δ is measured relative to the mirror plane at the point of observation (B, λ).

Let

B = magnetic field at magnetic latitude λ,

h = altitude of observation,

B_m = magnetic field at mirror point,

h_m = altitude of mirror point,

ℓ = distance of B_m below B, as measured along field line,

I = magnetic dip angle, and

r = dipolar radius.

The observed pitch-angle distribution, $f(\delta)\,d\delta$, is the product of

(a) the probability $p_1(\delta)$ that a particle has a pitch angle between δ and $\delta + d\delta$, and

(b) the probability $p_2(\delta)$ that this particle is detected by the observer.

In the following we shall assume a small-angle approximation for δ, valid for low altitudes, with B given by a magnetic dipole, and that the rate of particle injection into this limited region is constant.

Consider (a). We assume

$$p_1(\delta)\,d\delta \propto [\rho(\ell)]^{-1}\,\frac{d\ell}{d\delta}\,d\delta. \tag{6}$$

The relationship between pitch angle δ and ℓ is obtained from the expressions for the invariance of the magnetic moment and $B(\lambda)$.

Mirror equation:

$$\frac{\cos^2\delta}{B} = \frac{1}{B_m}, \tag{7}$$

from which (since B = constant)

$$2 \tan \delta \, d\delta = dB_m/B_m. \tag{8}$$

Dipole field:

$$B_m = B_0 (1 + 3 \sin^2\lambda_m)^{1/2} \cos^{-6}\lambda_m$$

and

$$dB_m/B_m = 3 \tan\lambda_m \frac{(3+5 \sin^2\lambda_m)}{(1+3 \sin^2\lambda_m)} d\lambda_m. \tag{9}$$

From equation 8 and 9:

$$\frac{d\lambda_m}{d\delta} = \frac{2 \tan \delta(1+3 \sin^2 \lambda_m)}{3 \tan \lambda_m(3+5 \sin^2 \lambda_m)} . \tag{10}$$

We now relate ℓ with δ:

$$\frac{d\ell}{d\delta} = \frac{r}{\cos I} \frac{d\lambda_m}{d\delta} . \tag{11}$$

Under the assumption that δ is small, $\tan\delta \approx \delta$, $I_m \approx I$, and using the relation $\tan I_m = 2 \tan\lambda_m$, we have

$$\frac{d\ell}{d\delta} = \frac{4}{3} r[(2 + \cos^2 I) \sin I]^{-1} \delta, \tag{12a}$$

$$\therefore \ \ell = \frac{K\delta^2}{2}, \tag{12b}$$

where

$$K \sin I = (4/3)\, r\,(2 + \cos^2 I)^{-1}. \tag{12c}$$

Hence, probability $p_1(\delta)\, d\delta$ is

$$p_1(\delta)\, d\delta \propto \left[\rho(\ell)^{-1} \frac{d\ell}{d\delta}\right] d\delta \propto K\delta \left[\rho(\delta)\right]^{-1} d\delta. \tag{13}$$

(b) The probability $p_2(\delta)$ that a particle is observed in increment dx along the field line is proportional to the product of the time it spends in dx, i.e., $\tau \propto dx/v_{\|} = dx/v\delta$, and the frequency of its bounce period $\nu \propto v$ [Hamlin et al., 1961]:

$$p_2(\delta) = \text{constant} \times \delta^{-1}.$$

Thus, pitch-angle distribution is

$$\begin{aligned} f(\delta)\, d\delta &= p_1(\delta)\, p_2(\delta)\, d\delta \\ &= c[\rho(\delta)]^{-1}\, d\delta. \end{aligned} \tag{14}$$

The pitch-angle distribution is therefore given by the inverse of the effective atmospheric density when expressed in terms of the pitch angle, δ.

Examples:

1. Exponential atmosphere: Scale height H is constant. At altitude h_m effective atmospheric density is of the form

$$\rho = \rho_0 \exp(-h_m/H),$$

$$h_m = h - \ell \sin I = h - (1/2)\, K \sin I\, \delta^2,$$

where h = altitude of observation,

$$\rho(\delta) = \rho(h) \exp\left(\frac{+K \sin I}{2H}\, \delta^2\right).$$

Thus

$$f(\delta)\, d\delta \propto \exp\left(\frac{-K \sin I}{2H}\, \delta^2\right) d\delta. \tag{15}$$

For an exponential atmosphere, the pitch-angle distribution is a Gaussian function whose variance is

$$\sigma^2 = H/(K \sin I)$$
$$= \frac{3}{4}\, \frac{H}{r}\, (2 + \cos^2 I). \tag{16}$$

In the South Atlantic anomaly at 400 km altitude, $r \approx 6800$ km, $H = 80$ km, $\cos I = 0.74$. Standard deviation of distribution is then $\sigma = 8.6°$.

2. Power-Law Atmosphere: Exponent n is constant.

Here,

$$\rho = \rho_0 (h_m/h)^{-n} = \rho_0 \left(1 - \frac{\ell \sin I}{h}\right)^{-n},$$

and the pitch-angle distribution becomes

$$f(\delta)\, d\delta \propto \left(1 - \frac{K \sin I}{2h}\, \delta^2\right)^n d\delta. \tag{17}$$

We note that equations 15 and 17 are equal to first order when $H = h/n$.

APPENDIX II. Average Minimum Mirror-Point Altitude

The time-integrated flux data that are recorded by the emulsion detectors during each satellite flight are dependent upon the orbital parameters such as altitude, inclination, and eccentricity. In order to correlate data from a number of different experiments, we adopted a flux-weighted, average minimum mirror-point altitude, $\bar{h}_{min}$, as the characteristic altitude for a given flight experiment. The altitude $\bar{h}_{min}$ is defined by the expression

$$\bar{h}_{min} = \frac{\sum_i f_i h_i}{\sum f_i} . \qquad (18)$$

To calculate $\bar{h}_{min}$ we compute B and L values for the satellite ephemeris at 1- minute intervals in the region of the South Atlantic anomaly. We use the Jensen and Cain geomagnetic field model [Jensen and Cain, 1962] to compute (B_i, L_i) and the corresponding minimum mirror-point altitude, $h_i(B_i, L_i)$. This value of h_i is then weighted by $f_i(B_i, L_i)$, the flux of trapped protons at (B_i, L_i) as given by the Injun 3 flux contours [Valerio, 1964].

For the ephemerides we are considering here, $\bar{h}_{min}$ is less than the altitude of the satellite at the site of maximum flux (34° S, 34° W), by an amount Δh = 20 to 45 km. The correction Δh increases approximately in proportion to altitude.

We have used $\bar{h}_{min}$ as a principal parameter to analyze our data, and it is pertinent to examine the dependence of the altitude-flux profile (Figure 6) upon the particular choice of B-L flux contour to compute $\bar{h}_m$. For this examination we used the Injun 3, 1964-45A, and Telstar I B-L proton flux contours. Table I summarizes the results of this analysis.

Tabulated are the input models (flux and field used to compute $\overline{h}_{min}$, and the power-law coefficients obtained by a least-squares analysis of the data.

The least-squares results given in Table I illustrate that a power-law behavior accurately describes the flux-altitude profile. Irrespective of the flux model used to compute $\overline{h}_{min}$, a power-law relation orders our flux-vs-altitude data to accuracies 7.8 per cent to 8.9 per cent. The Injun 3 and 1964-45A B-L contours are of similar shape, and give values of $\overline{h}_{min}$ that agree within ±1 km. The differences between the resultant altitude profiles are therefore negligible. Relative to the Injun 3 and 1964-45A data, the Telstar I flux contours differ sufficiently to affect systematic, altitude-dependent differences in $\overline{h}_{min}$, which in turn produce a slightly steeper altitude-flux profile.

Because the B-L proton flux contours listed in Table I are based upon the Jensen and Cain 48-coefficient field, it is not possible to check directly the effects different magnetic field models have upon the data given in Figure 6. That such effects are probably small is evidenced by the fact that when we use the Injun 3 data to weight the $\overline{h}_{min}$ values obtained from the GSFC (9/65) 99-coefficient field model [Hendricks and Cain, 1966] we find the resulting altitude profile is identical to that obtained for the Injun 3 48-coefficient combination given in Table I.

Table I. Results of the least-squares analysis of the observed omnidirectional proton flux detected per day during ascending-node traversals of the South Atlantic anomaly, versus $\overline{h}_{min}$. The B-L flux and field models used to compute $\overline{h}_{min}$ are designated. The functional form is $J(63\ MeV) = a\ \overline{h}_{min}^{n}$. The goodness of the LS fit is given by σ (SD), the per cent standard deviation in the experimental data about the least-squares power-law fit.

$\overline{h}_{min}$		log a	n	σ (SD) (per cent)
Flux	Field			
Injun 3	JC	-8.29 ±0.20	4.67 ±0.08	7.6
1964-45A	JC	-8.26 ±0.21	4.66 ±0.08	8.1
Telstar I	JC	-9.05 ±0.25	4.97 ±0.10	8.9

REFERENCES

Armstrong, A. H., F. B. Harrison, H. H. Heckman, and L. Rosen, Charged particles in the inner Van Allen radiation belt, J. Geophys. Res., 66, 351-357, 1961.

Barkas, W. H., Nuclear Research Emulsions, Chapt. 9, Academic Press, New York and London, 1963.

Blanchard, R. C., and W. N. Hess, Solar cycle changes in inner-zone protons, J. Geophys. Res., 69, 3927-3938, 1964.

CIRA 1965 (COSPAR International Reference Atmosphere 1965), North-Holland, Amsterdam, 1965.

Dragt, A. J., Effect of hydromagnetic waves on the lifetime of Van Allen radiation protons, J. Geophys. Res., 66, 1641-1649, 1961.

Dragt, A. J., M. M. Austin, and R. S. White, Cosmic ray and solar proton albedo neutron decay injection, J. Geophys. Res., 71, 1293-1304, 1966.

Farley, T. A., and N. L. Sanders, Pitch angle distribution and mirror point densities in the outer radiation zone, J. Geophys. Res., 67, 2159-2168, 1962.

Filz, R. C., Observations of inner-zone protons in nuclear emulsions 1961 to 1966, Earth's Particles and Fields, edited by B. M. McCormac, pp. 15-22, Reinhold Book Corporation, New York, 1968.

Filz, R. C., and E. Holeman, Time and altitude dependence of 55-MeV trapped protons, August 1961 to June 1964, J. Geophys. Res., 70, 5807-5822, 1965.

Freden, S. C., J. B. Blake, and G. A. Paulikas, Spatial variation of the trapped proton spectrum, J. Geophys. Res., 70, 3113-3116, 1965.

Freden, S. C., J. B. Blake, and G. A. Paulikas, private communication, 1967.

Freden, S. C., and R. S. White, Protons in the earth's magnetic field, Phys. Rev. Letters, 3, 9-10, 1959.

Freden, S. C., and R. S. White, Particle fluxes in the inner radiation belt, J. Geophys. Res., 65, 1377-1383, 1960.

Freden, S. C., and R. S. White, Trapped proton and cosmic-ray albedo neutron fluxes, J. Geophys. Res., 67, 25-29, 1962.

Gabbe, J. D. and W. C. Brown, Some observations of the distribution of energetic protons in the earth's radiation belts between 1962 and 1964, Radiation Trapped in the Earth's Magnetic Field, B. M. McCormac, Editor, pp. 165-184, D. Reidel Publishing Company, Holland, 1966.

Galperin, Yu. I., and V. V. Temny, Atmospheric scale height in the 200-400 km range according to radiation belt data, Space Research V, 769-778, 1965.

Garmire, G., Geomagnetically trapped protons with energies greater than 350 MeV, J. Geophys. Res., 68, 2627-2638, 1963.

Hamlin, D. A., R. Karplus, R. C. Vik, and K. M. Watson, Mirror and azimuthal drift frequencies for geomagnetically trapped particles, J. Geophys. Res., 66, 1-4, 1961.

Harris, I., and W. Priester, Theoretical models for the solar cycle variation of the upper atmosphere, J. Geophys. Res. 67, 4585-4591, 1962. Also National Aeronautics and Space Administration Technical Note No. D-1444, 1962 (unpublished).

Harris, I., and W. Priester, Relation between theoretical and observational models of the upper atmosphere, J. Geophys. Res., 68, 5891-5894, 1963.

Heckman, H. H., and A. H. Armstrong, Energy spectrum of geomagnetically trapped protons, J. Geophys. Res. 67, 1255-1262, 1962

Heckman, H. H., and V. O. Brady, Effective atmospheric losses for 125-MeV protons in South Atlantic anomaly, J. Geophys. Res., 71, 2791-2798, 1966.

Heckman, H. H., and G. H. Nakano, East-West asymmetry in the flux of mirroring geomagnetically trapped protons, J. Geophys. Res., 68, 2117-2120, 1963. See also postdeadline paper, AGU meeting, Dec. 27-29, 1962, in Trans. Am. Geophys. Union, 44(1), 205, 1963.

Heckman, H. H., and G. H. Nakano, Direct observations of mirroring protons in the South Atlantic anomaly, Space Research V, 329-342, 1965.

Hendricks, S. J., and J. C. Cain, Magnetic field data for trapped particle evaluations, J. Geophys. Res., 71, 346-347, 1966.

Jensen, D. C., and J. C. Cain, An interim geomagnetic field (abstract), J. Geophys. Res., 67, 3568-3569, 1962.

King-Hele, D. G., and J. Hingston, Air density at heights near 190 km in 1966-1967, from the orbit of Secor 6, Planet. Space Sci., 16, 675-691, 1968 a.

King-Hele, D. G., and J. Hingston, Variations in the air density at 480 km, from the orbit of Midas 2, Planet. Space Sci., 16, 937-949, 1968 b.

Lenchek, A. M., and S. F. Singer, Effects of the finite gyroradii of geomagnetically trapped protons, J. Geophys. Res, 67, 4073-4075, 1962.

McIlwain, C. E., and G. Pizzella, On the energy spectrum of protons trapped in the earth's inner Van Allen zone, J. Geophys. Res., 68, 1811-1824, 1963.

Nakano, G. H., and H. H. Heckman, Evidence for solar-cycle changes in the inner-belt protons, Phys. Rev. Letters, 20, 806-809, 1968.

Northrop, T. G., Adiabatic charged-particle motion, Rev. Geophys. 1, 283-304, 1963.

Patrick, J. W., and W. H. Barkas, The grain density of emulsion tracks, Nuovo Cimento (Supplemental), 23, 1-16, 1962.

Peterson, L. E., private communication, 1966.

Valerio, J., Protons from 40 to 110 MeV observed on Injun 3, J. Geophys. Res. 69, 4949-4958, 1964.

Vette, J. I., Models of the trapped radiation enviroment, Vol. I: Inner zone protons and electrons, NASA SP-3024, 1966.

FIGURE CAPTIONS

Fig. 1. Photograph of emulsion detectors (A-D) mounted on satellite ballast shell. Coordinates $\hat{i}\,\hat{j}\,\hat{k}$ are fixed in the satellite frame. During flight $\hat{i}$ is oriented toward the zenith and $\hat{k}$, the axis of symmetry of the satellite, is in the orbital plane.

Fig. 2. Mean orientation of mirror planes as recorded by emulsion detectors for an orbit inclination of 75°. Detectors A-D are represented by disks that are tangent to hemispherical shell. The plane whose normal is directed to the right of the illustration is the ascending-node plane. The normal to the descending-node plane is toward the upper left. In this illustration, the observer's line of sight is close to the descending-node plane.

Fig. 3. Geographic coordinates of the site of mirroring particles in the South Atlantic anomaly as determined in this experiment. Each point is for a separate satellite flight. Error bars represent the statistical errors in the site locations. Magnetic declination and inclination angles are respectively indicated by solid and dashed lines.

Fig. 4(a). Proton-flux scale height, H, versus altitude, $\overline{h}_{min}$, from east-west asymmetry measurements. Data are compared with the calculations of Heckman and Brady [1966], given by the solid lines labeled S = 100 and 200. Dashed lines are least-squares fits to east-west asymmetry data (n = 4.93) and the altitude-vs-flux data (n = 4.67).

(b). Power-law exponent n as derived from east-west asymmetry measurements.

Fig. 5. Scanning geometry for stack A. Here, $\underset{\sim}{B}$ is approximately along $\hat{y}$. The mirror plane is nearly coincident with the $\hat{x}$ - $\hat{z}$ plane. The vector $\underset{\sim}{B} \times \hat{r}$ is the eastward direction, $\phi = 0$. Measured is the vertically incident flux of stopping protons ($\underset{\sim}{P}$) whose projected angle on the mirror plane is $\phi_p \leq \pm 15°$. The azimuthal angle between the east-west and mean incident directions is ϕ_v.

Fig. 6. Omnidirectional flux, J(63 MeV) cm^{-2} MeV^{-1} day^{-1}, versus altitude, $\overline{h}_{min}$. Data from this experiment are shown as open circles. The least-squares fit to the data is given by the solid line, J_c. The corresponding Injun 3 computed fluxes and least-squares fit are shown by the solid points and dashed line.

Fig. 7. Proton energy spectra, E > 57 MeV, 6/63 to 6/66. Dashed curve is from data taken in 1960, normalized to the present data at E = 63 MeV [Heckman and Armstrong, 1962].

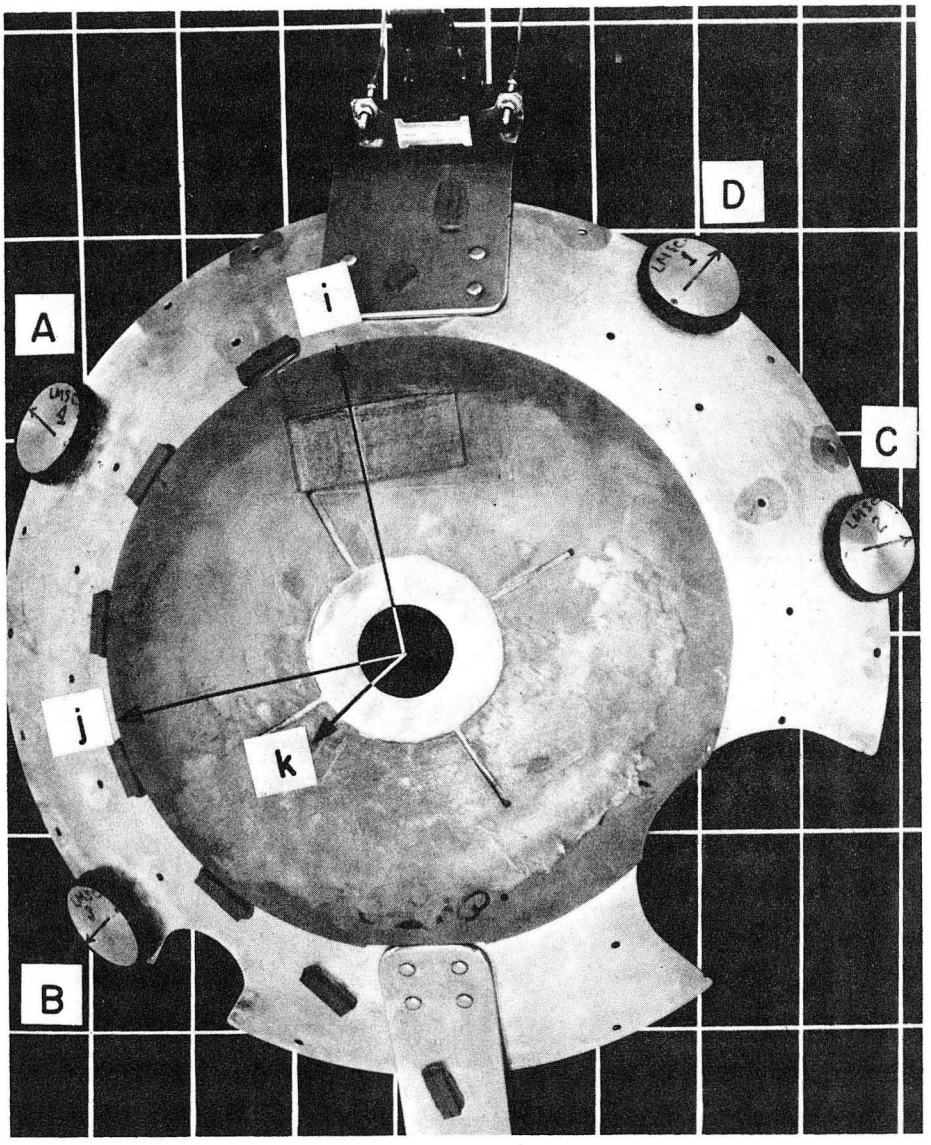

XBB 689-5640

Fig. 1

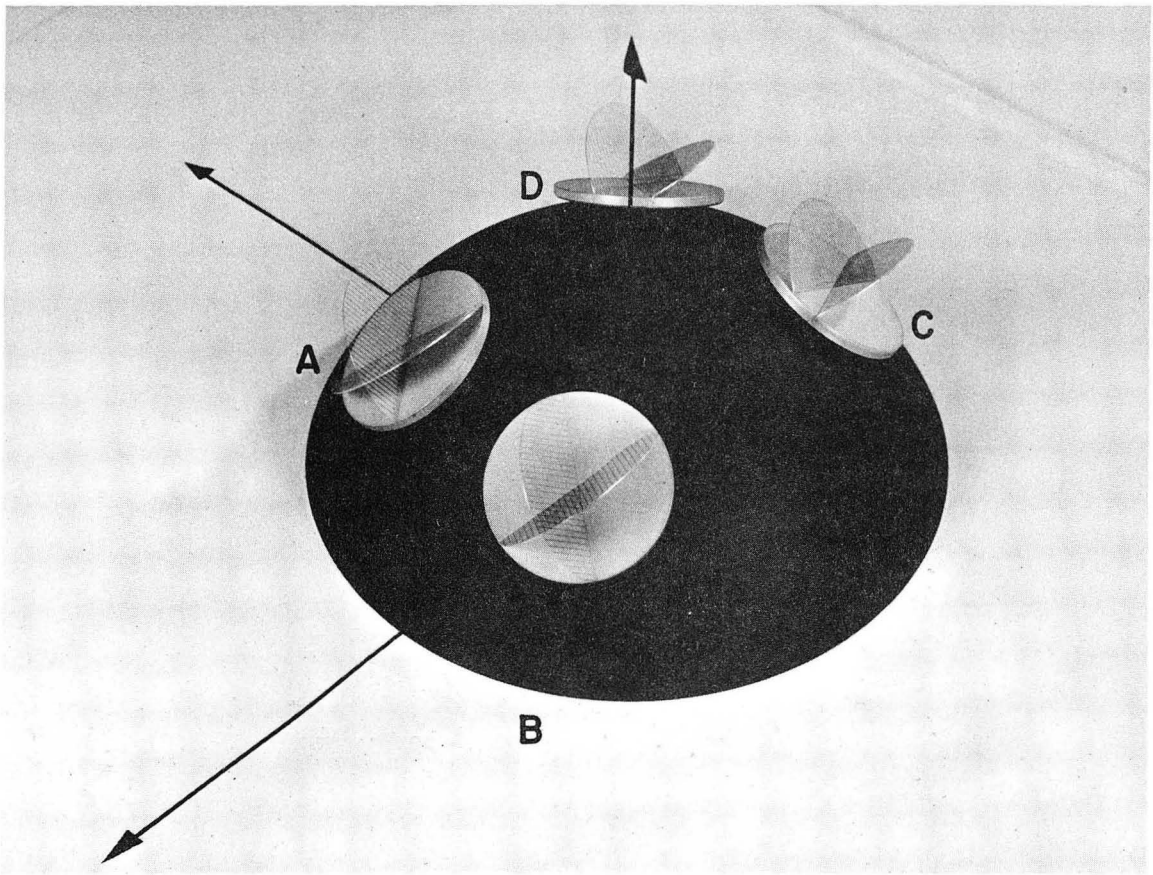

XBB 689-5639-A

Fig. 2

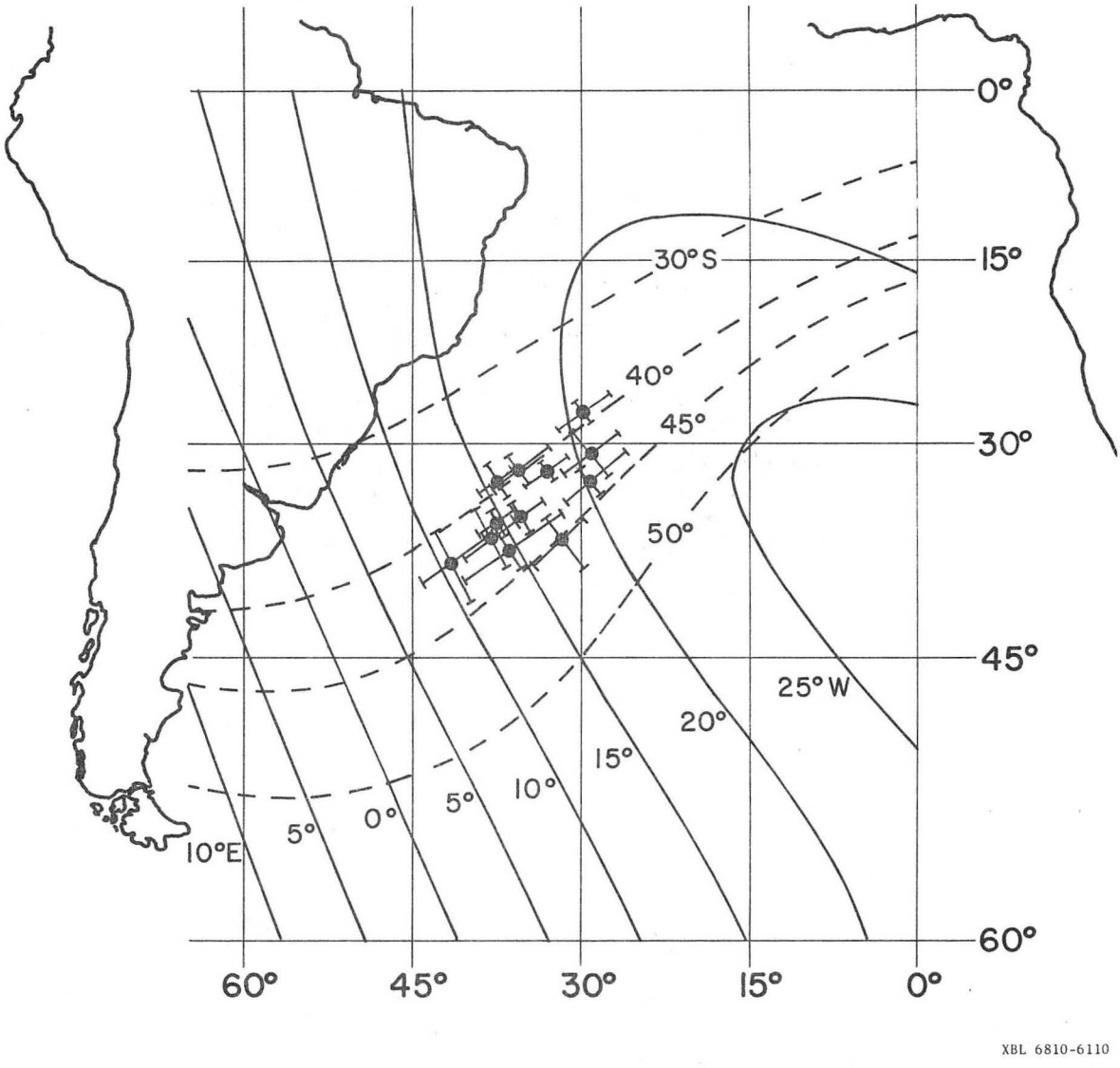

XBL 6810-6110

Fig. 3

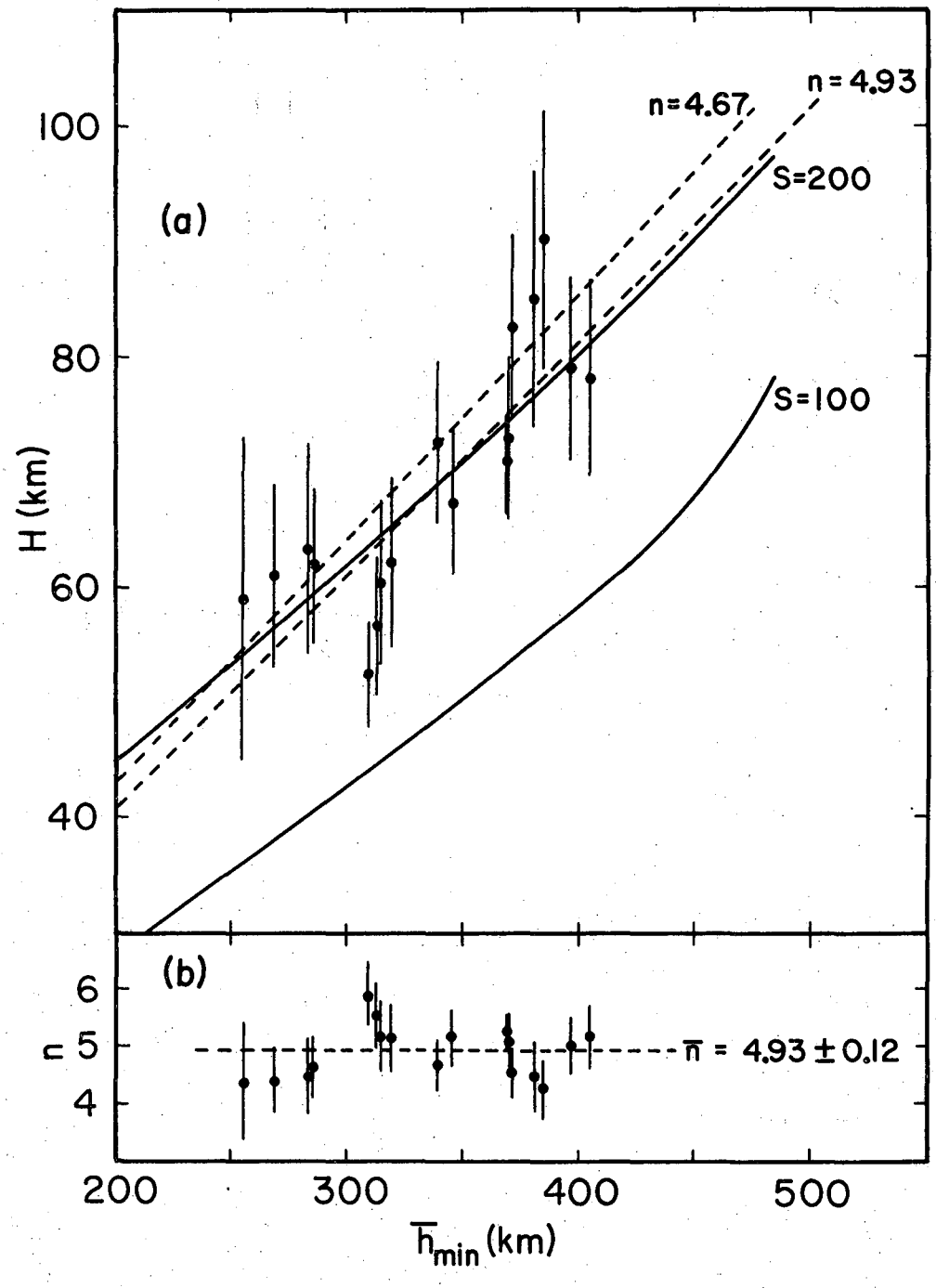
n=4.67
n=4.93
S=200
S=100
(a)
H (km)
100
80
60
40
(b)
n
6
5
4
$\bar{n}$ = 4.93 ± 0.12
200
300
400
500
$\bar{h}_{min}$ (km)
XBL 6810-6111

Fig. 4

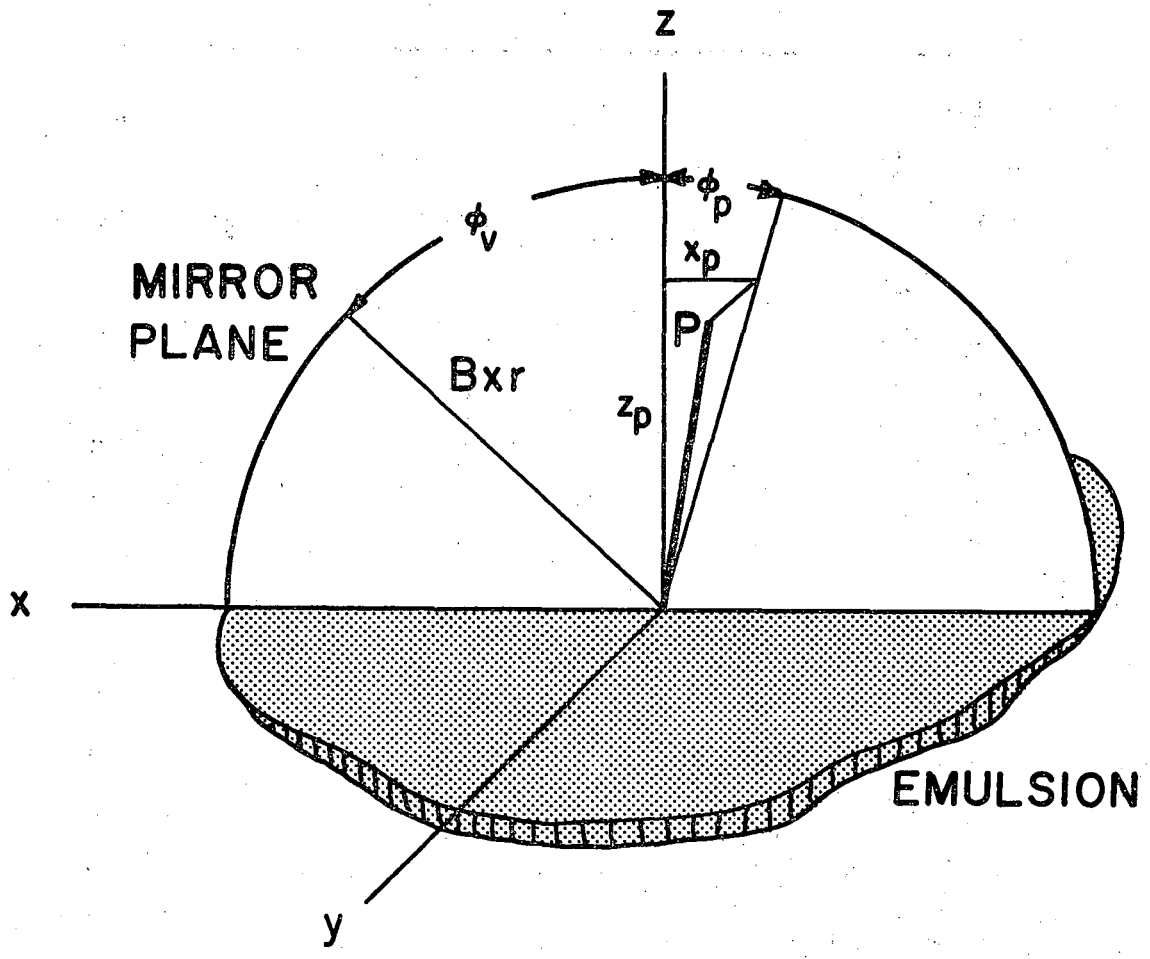

XBL 6810-6112

Fig. 5

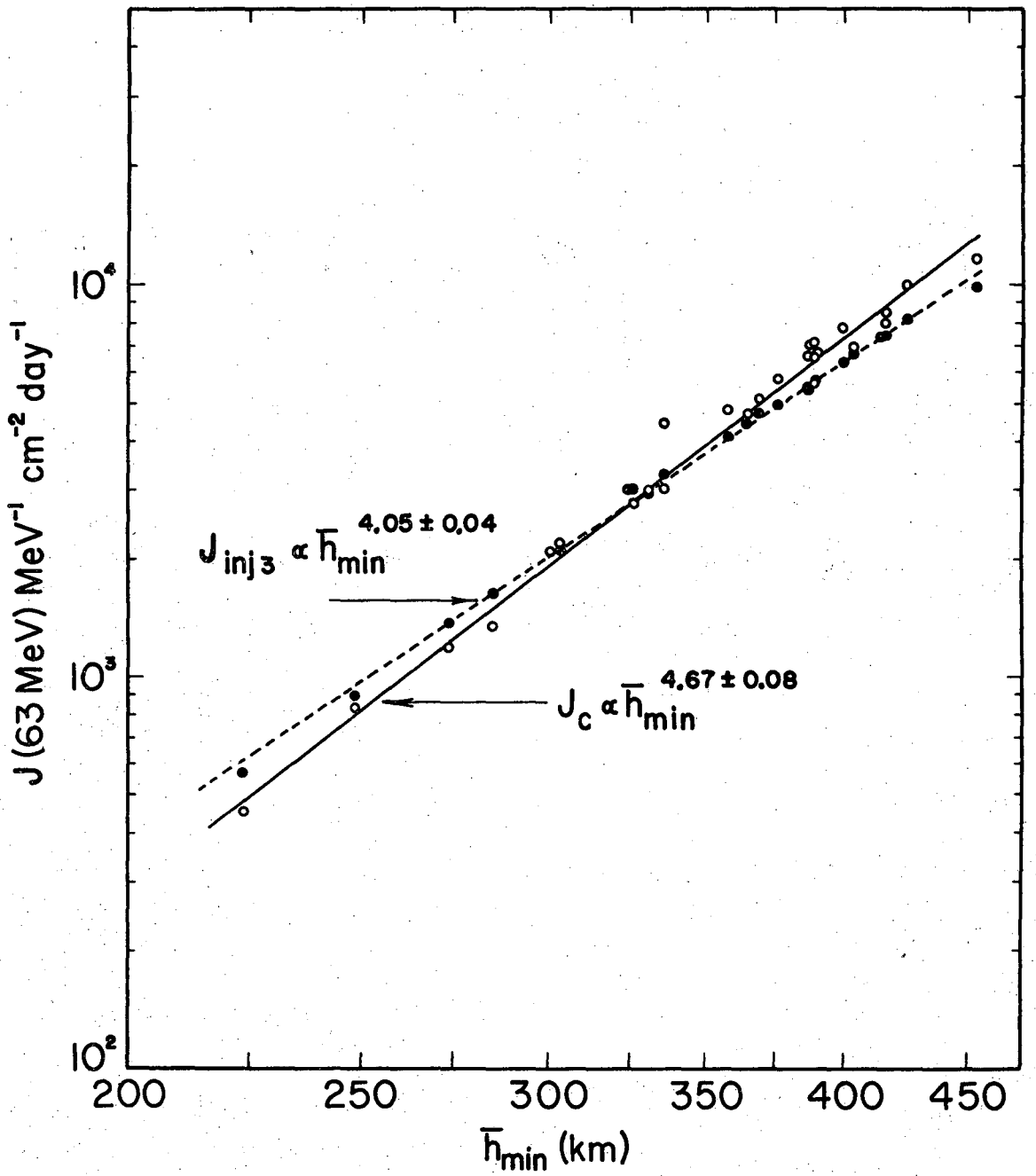

XBL 6810-6113

Fig. 6

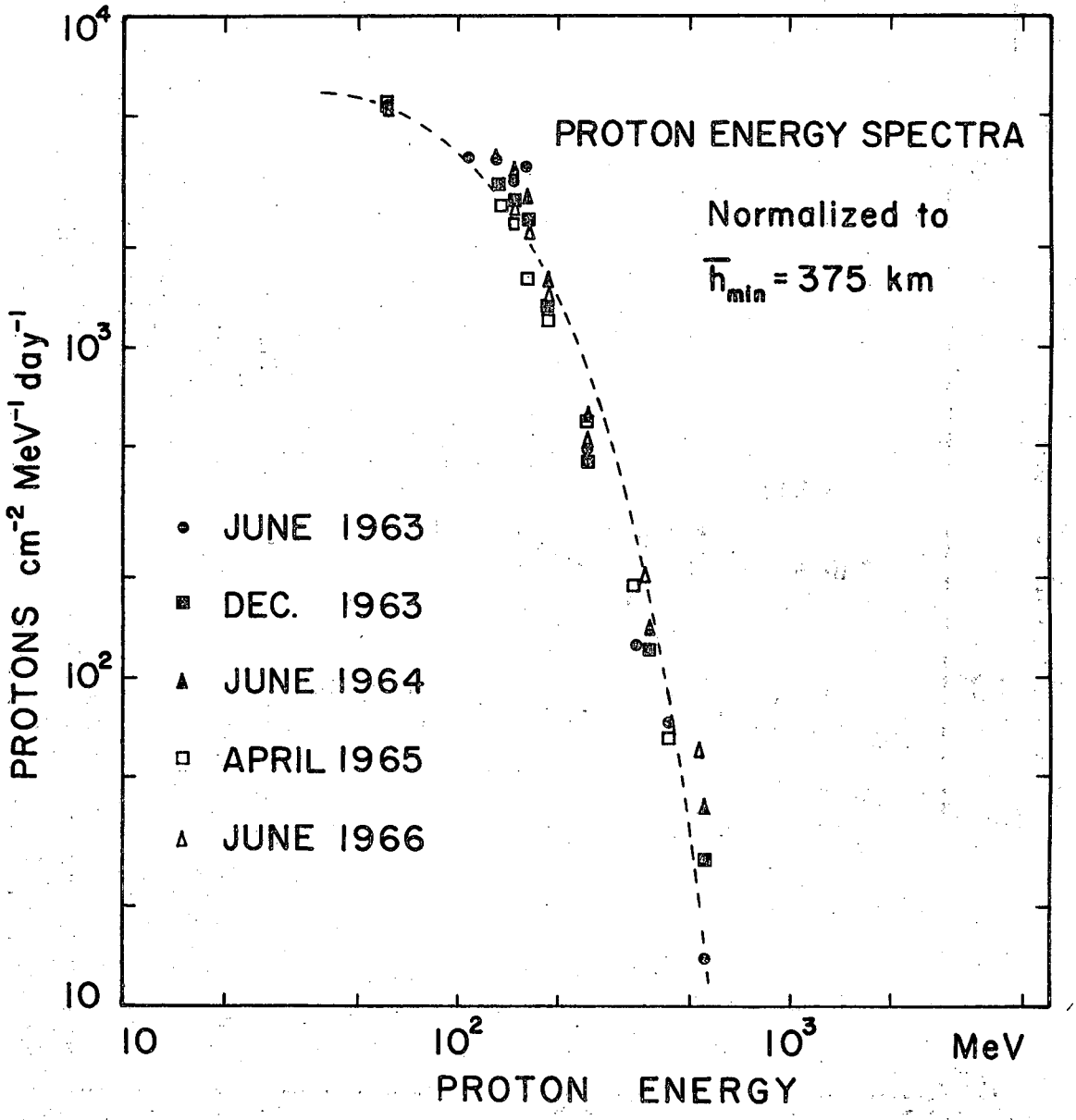

XBL 6810-6114

Fig. 7

LEGAL NOTICE

TECHNICAL INFORMATION DIVISION
LAWRENCE RADIATION LABORATORY
UNIVERSITY OF CALIFORNIA
BERKELEY, CALIFORNIA 94720